Water Air Soil Pollut (2024) 235:572
https://doi.org/10.1007/s11270-024-07371-3

Histidine-Functionalised Polypyrrole Hybrid Nanocomposite for Adsorption of Toxic Hexavalent Chromium from Water

Marko Chigondo · Benias Nyamunda · Munashe Maposa · Knowledge Nyenyayi · Delroy Nyadenga · Fidelis Chigondo

Received: 21 November 2022 / Accepted: 18 July 2024 / Published online: 5 August 2024

Abstract Chromium(VI) is one of the most toxic metal ions as it can bioaccumulate and its excessive assimilation may result in anaemia, nervous system failure, kidney damage, cancers of the digestive tract and lungs. In this study a polypyrrole (PPy) modified with histidine (His) by in situ polymerisation technique was investigated for the removal of Cr(VI) from aqueous and characterised by means of Fourier transform infrared (FTIR) spectroscopy, X-ray diffraction (XRD), field emission scanning electron microscopy/energy dispersive X-ray spectroscopy (FE-SEM/EDS), high resolution-transmission electron microscopy (HR-TEM) and X-ray photoelectron spectroscopy (XPS).The influence of solution pH, adsorption time, initial adsorption concentration, temperature and coexisting ions on its adsorption were investigated. The results showed that the optimum adsorption pH was 2.0 with the adsorption being endothermic and chemisorption in nature. Mono-layer adsorption was witnessed as the Langmuir isotherm best described the process with a maximum adsorption capacity 274.73 mg g^{-1} at 25 °C. Although the removal of Cr(VI) was the primary drive, the reduction of Cr(VI) to Cr(III) during treatment turned out to be very significant to avoid secondary pollution. The adsorption mechanisms were mainly ion exchange, electrostatic attractions, complexation, chelation reactions with protonated histidine sites and reduction. Remarkably, the His-PPy nanocomposite exhibited an exceptional removal for Cr(VI) ions after three cycles of adsorption–desorption (over 99%) suggesting the adsorbent's exceptional recyclability. The adsorption equilibrium was attained from 60 to 150 min and best described by pseudo-second-order kinetics. The high adsorption efficiency, stability and selectivity makes the His-PPy nanocomposite adsorbent potentially suitable for large-scale Cr(VI) ions removal from water.

Keywords Histidine · Polypyrrole · Nanocomposite · Adsorption · Chromium (VI)

M. Chigondo (✉) · B. Nyamunda · M. Maposa · K. Nyenyayi · D. Nyadenga · F. Chigondo
Department of Chemical and Processing Engineering, Manicaland State University of Applied Sciences, Fern Hill Campus P. Bag 7001, Mutare, Zimbabwe
e-mail: marko.chigondo@staff.msuas.ac.zw; chigozma@gmail.com

M. Chigondo · B. Nyamunda · M. Maposa · K. Nyenyayi · D. Nyadenga · F. Chigondo
Department of Chemical Sciences, Midlands State University, P. Bag 9055, Gweru, Zimbabwe

1 Introduction

Hexavalent Chromium (Cr(VI)), one of the most common heavy metals ions are prominent in wastewater due to the wide range of sources associated with intensive industrial utilisation of chromium containing compounds and products in tanning, electroplating, paint and pigment

manufacture, mining operations among other areas (Baig et al., 2015, Chen et al., 2020, Deng et al., 2018, Katata-Serua et al., 2020). It is among the 20 global top-priority toxic pollutants (Chen et al., 2020). Besides being highly soluble, labile and mobile (Karthikeyan et al., 2021), Cr(IV) ions are non-biodegradable and bio-accumulate through the food chain (Katata-Serua et al., 2020). Their toxicity manifests by infiltration through cell membranes, initiating the development of unstable and highly reactive intermediates which are accountable for cells as well as DNA destruction, kidney damage and liver damage in human beings (Dutta et al., 2021; Pereira et al., 2021; Zhitkovich, 2011). According to World Health Organization (WHO) and United States Environmental Protection Agency (EPA), the maximum allowable limits of total chromium in drinking water are 0.05 and 0.1 mg L^{-1} respectively (Adeiga et al., 2022, Katata-Serua et al., 2020). This makes it imperative to eliminate Cr(VI) ions from the environmental waters hence the extensive search for technologies that can remediate this problem. On that note a manifold of technologies is available ranging from chemical precipitation, reverse osmosis, electrochemical, membrane filtration, ion exchange, microbiological treatment and adsorption (Das et al., 2019, Dinker et al., 2015, Mahmud et al., 2016, Maity et al., 2019).

Traditionally chemical precipitation has been used to treat Cr(VI) as it is an established technology, simple to operate and to some extent effective. Nonetheless, it produces chromium-containing sludge and requires large quantities of chemicals which are expensive (Liu et al., 2021). On the other hand, ion exchange is very selective and removes large amounts of pollutant but its operation and management are complex requiring huge initial investment. Microbiological treatment has low processing costs, little secondary pollution and purifies the milieu while eliminating chromium. However, the toxicity tolerance of organisms to Cr(VI) ions is restricted and therefore the process has limitations besides the problems of microbes management and sustainability (Liu et al., 2021). Reverse osmosis, electrochemical treatment, membrane filtration and photocatalytic treatment are other methods available but these suffer a setback of high investment, technical expertise, post-treatment requirement, are energy intensive and result in fouling (Cheng et al., 2021, Zhou et al., 2018). In comparison to the aforementioned techniques adsorption has been found to be exceptionally convenient in Cr(VI) ions removal, attributable to its simplicity, ease of operation, minute by-products and economic sustainability (Li et al., 2020, Liu et al., 2021, Wei et al., 2020, Zhou et al., 2018). To this end, several adsorbents have been studied and reviewed, ranging from polymers, graphene materials, carbon nanotubes, biomaterials, alumina, silica and binary nanometal oxides (Dinker et al., 2015, Du et al., 2020, Li et al., 2020). However, numerous challenges have been encountered during their utilisation such as tedious and expensive methods of preparation, generation of additional solid wastes, low adsorption capacities owing to the low specific surface areas and unavailability of active functional groups (Dinker et al., 2015, Du et al., 2020, Li et al., 2020, Liu et al., 2018).

Lately PPy-based adsorbents have become more popular in water treatment ascribed to easy synthesis, cost-effectiveness, environmental stability and outstanding ion exchange and redox properties (Du et al., 2020; Liu et al., 2018; Wang et al., 2020). Pristine PPy has little adsorption ability for Cr(VI) ions due to its tendency to agglomerate, attributed to π-π interactions between the chains leading to reduced surface area (Chigondo et al., 2019; Kera et al., 2016). However, researchers have started to pay attention to the designs aimed at significantly improving its Cr (VI) adsorption properties by doping with amino containing groups like glycine, arginine, diamino sulphonic acid, and theorene (Amalraj et al., 2016a, Ballav et al., 2012, Chigondo et al., 2019, Kera et al., 2018). Several studies have been reported in this respect namely (PPy-arginine) (Chigondo et al., 2019), PPy-PANI nanofibers (Bhaumik et al., 2012), (Polypyrrole-coated gum ghatti-grafted poly (acrylamide) (Goddeti et al., 2020), PPy-glycine (Ballav et al., 2012), PPy-NH_2 (Liu et al. 2017), PANI-PPy/Fe_3O_4, 2.5- diaminosulphonic acid-PPy and *m*-Phenylenediamine-modified PPy) (Kera et al., 2016, 2017, 2018), PPy-PANI/Fe_3O_4 arginine-doped polyaniline/walnut shell (Hsini et al., 2020), Thr-PPy and Asp/PPy (Amalraj et al., 2016a and 2016b) and 4-amino-3-hydroxynaphthalene-1-sulfonic acid doped PPy (Sall et al., 2017). These studies utilised amino dopants to enhance PPy adsorption of Cr(VI) successfully as targeted design and fabrication of composite adsorbents with high adsorption and

reduction properties help to compensate for the inadequate PPy adsorption capacity.

Amino-based dopants have strong Cr(VI) ions affinity and are exceptionally selective towards the direct absorption of Cr(VI) ions and subsequent reduction to Cr(III) on adsorption sites. This is accomplished by donation of electrons by O, S and N atoms of dopants forming metal complexes or chelates (Ates et al., 2012; Li et al., 2020; Rodríguez et al., 2000; Wang et al., 2022). Based on the aforementioned advantages, this work combines with surface functionality to design a novel amino-functionalized efficient for Cr(VI) removal from polluted water and there is still ample scope to explore other amino dopants. Thus the study aimed to synthesise histidine-doped polypyrrole hybrid adsorbent and evaluate its capacity to remove Cr(VI) ions from water. The nitrogen atoms of these adsorbents turn into electron donors for the Cr(VI) reduction to Cr(III) under acidic conditions and offer the adsorption sites for Cr(III) besides Cr(VI). This occurs through electron transfer from a neutral state (PPy^0) to Cr(VI) (Fang et al., 2018). The histidine amino acid contains three nitrogen atoms per molecule therefore it is envisaged that increasing the number of functional groups in the histidine-doped polypyrrole hybrid adsorbent would produce an adsorbent with even higher adsorption capacity and multi-functional properties. Cost-effective functional materials having multifunctional active sites for both adsorption and Cr(VI) reduction would be essential for hands-on applications. Thus histidine-doped polypyrrole (His-PPy) hybrid adsorbent could be a novel adsorbent for Cr (VI) ions adsorption.

The objectives of this study were to fabricate histidine-doped polypyrrole hybrid adsorbent by in situ polymerisation and characterised the as-synthesised adsorbent was through FTIR, XRD, SEM–EDS, HR-TEM and XPS techniques. Batch adsorption experiments on the effectiveness of the His-PPy adsorbent on Cr(VI) ions were evaluated through the effect of adsorbent dosage, pH, initial concentration, temperature, contact time and co-existing ions. Industrial effluent laden with Cr(VI) ions was tested to evaluate the potential applicability of His-PPy on real field samples and comparison with other adsorbents. Moreover, the recyclability of His-PPy was assessed through the adsorption–desorption cycles study.

2 Materials and Methods

2.1 Materials

Pyrrole (Py), l-histidine (His) and ammonium persulphate (APS) were purchased from Sigma-Aldrich South Africa with the pyrrole monomer being distilled before use. Hydrochloric acid (HCl), acetone (C_3H_6O), sodium hydroxide (NaOH), potassium dichromate ($K_2Cr_2O_7$) and 15-diphenyl carbazide of analytical grades were obtained from Sigma-Aldrich USA and used without further treatment.

2.2 Fabrication of His-PPy Composites

The His-PPy hybrid composite was synthesized by in situ interfacial polymerisation of freshly distilled pyrrole in which varying amounts (1.1, 1.2 and 1.3 g) of l-histidine were introduced under ultrasonic vibration over 1 h (Ballav et al., 2014; Bhaumik et al., 2012). Subsequently APS (3.9 g) was dissolved in 20 mL of deionised water and added dropwise to each mixture. The solution mixtures were continuously stirred for an additional 20 min. The resulting solution was left for 12 h at ambient temperature after which 10 mL of acetone was added to stop the polymerisation process. The dark black suspensions were carefully separated by filtration followed by washing with acetone and distilled water and the precipitates were oven dried overnight at 80 °C to afford the His-PPy nanocomposites (Chigondo et al., 2019).

2.3 Characterisation of His-PPy Nanocomposite

The FTIR spectra of the pristine PPy and His-PPy nanocomposite were measured over 500–4000 cm^{-1} in a resolution of 4 cm^{-1} by means of a Perkin Elmer Spectrum 100 Spectrometer (Perkin Elmer USA) with 32 scans. The FE-SEM and TEM images of the His-PPy nanocomposite were established through use of a Zeiss Auriga Cobra FIB microscope and a high-resolution transmission electron microscope (JEOL–JEM 2100 Japan) with LaB6 filament operated at 200 kV

respectively. A D2-advance X-ray diffractometer (Bruker, Germany) at 2θ from 5° and 90° (scan rate 5°/min) using CuKα of wavelength of 1.5505 Å and adaptable slits at 45 kV/30 mA was used for measuring XRD patterns. The XPS analysis of adsorbents was studied using a Kratos Axis Ultra device with Al monochromatic X-ray source (1486.6 eV).

2.4 Batch Adsorption Studies

A stock solution containing 1000 mg/L Cr(VI) ions was prepared using 2.830 g of oven dried $K_2Cr_2O_7$ dissolved in 1000 mL of deionised water. Appropriate serial dilutions of this stock solution produced the required experimental solutions for Cr(VI) ions removal studies. Triplicate studies were carried out by contacting 0.05 g of His-PPy adsorbent with 50 mL of 200 mg/L Cr(VI) ions solutions which were agitated in a temperature-controlled water bath shaker at 200 rpm for 24 h thus the adsorption data in the discussion has the error bars representing the standard deviation. The residual Cr(VI) ions determination in treated water samples was conducted by measuring the absorbance of the purple Cr(VI) complex with 15-diphenyl carbazide reagent at 540 nm.

The removal percentage of Cr (VI)ions was determined using Eq. (1):

$$Removal\ \% = \left(\frac{C_o - C_e}{C_o}\right) \times 100 \quad (1)$$

where C_o and C_e are the initial and equilibrium Cr(VI) concentration respectively. The effect of adsorbent dosage was studied by varying the amounts of the adsorbent from 0.01 to 0.07 g on the removal of 200 mg L^{-1} of Cr(VI) ions solution at optimised pH 2. The equilibrium adsorption capacity of the adsorbent is given by Eq. (2):

$$q_e = \left(\frac{C_o - Ce}{m}\right) V \quad (2)$$

where q_e (mg g^{-1}) and V (L) represent the equilibrium amount of Cr(VI) ions per unit mass of adsorbent and the solution volume respectively.

To fully understand the adsorption process and adsorption mechanism, adsorption isotherms were explored at 15, 25, 35 and 45 °C solution temperatures with 50–500 mg L^{-1} initial Cr(VI) ions concentration, 0.05 g adsorbent dosage and pH 2. The isotherm data associated with the adsorption process made it possible to establish the changes in thermodynamic parameters namely Gibbs free energy ($\Delta G°$), enthalpy ($\Delta H°$) and entropy ($\Delta S°$). Adsorption kinetics is crucial for predicting the rate and modelling of a water treatment process. To study determine this, 50 mL solutions of 50, 100 and 150 mg L^{-1} initial Cr(VI) ions concentrations at 25 °C, 0.05 g adsorbent dose and pH 2 were shaken for 0 to 300 min. The adsorption capacity of the adsorbent (q_t) at any given time was evaluated using Eq. (3):

$$q_t = (\frac{C_o - C_t}{m})V \quad (3)$$

where q_t (mg g^{-1}) and C_t (mg L^{-1}) represent the quantity of Cr (VI) ions taken per unit mass of adsorbent and the concentration of Cr (VI) ions at time t respectively.

2.5 Effect of Co-existing Ions

The study of the interference of co-existing ions on adsorption is essential since no ion exists isolated in water bodies. Henceforth, this was executed by dissolving precursor salts of the chloride (Cl^-), sulphate (SO_4^{2-}), nitrate (NO_3^-), hydrogen carbonate (HCO^-_3), phosphate (PO_4^{3-}), zinc ions (Zn^{2+}), copper ions (Cu^{2+}), nickel ions (Ni^{2+}), magnesium ions (Mg^{2+}), calcium ions (Ca^{2+}) and multi-ions at 0, 10, 20, 30 and 40 mg L^{-1} combined with at 0, 50, 100 and 150 mg L^{-1} solutions of Cr (VI) ions in deionised water. Subsequently the solutions were shaken using the optimised adsorbent dose at pH 2 for 24 h followed by analysis for the residual Cr(VI) ions.

2.6 Regeneration Studies

To investigate the reusability and stability of His-PPy, 0.05 g of the adsorbent was added to 50 mL of 200 mg L^{-1} Cr(VI) ions solution at pH 2. The Cr (VI) loaded adsorbent was shaken with 0.005, 0.025, 0.05 and 0.1 M NaOH solutions. The 0.1 M NaOH solution produced the highest desorption capability which was then applied for four consecutive desorption cycles with 2 M HCl employed for regeneration of the adsorbent.

3 Results and Discussion

3.1 Physico-chemical Characterisation

Figure 1A(a) and (b) display the FTIR of the His-PPy before and after Cr(VI) adsorption, whilst (c) shows the FTR spectra of pristine PPy. The characteristic peaks at 1527, 1437 and 961 cm^{-1} exposed by FTIR spectrum of pristine PPy are ascribed to the stretching vibrations of C=C, C–N and C–H deformations respectively (Amalraj et al., 2016a, Ballav et al., 2012, Chigondo et al., 2019, Karthikeyan et al., 2021, Wang et al., 2022). On the other hand, the band at 3131 cm^{-1} is attributed to N–H stretching vibration owing to the presence of $-{}^{+}NH_3$ function of the histidine zwitterion (Amalraj et al., 2016a and b, Ballav et al., 2012, Chigondo et al., 2019). The peaks at 1527 and 1437 cm^{-1} in pristine PPy shifted to 1539 and 1438 cm^{-1} respectively possibly as a result of histidine dopant incorporation in the PPy moiety (Ballav et al., 2014; Bhaumik et al., 2011; Kera et al., 2016; Wang et al., 2015). This band shift might be a result of interaction of the histidine amino acid with the PPy backbone which disrupts the PPy conjugate structure resulting in restricted degree of polymer chain charge delocalization (Xiang et al., 2021; Xu et al., 2019). Furthermore, after Cr (VI) ions adsorption most peaks became intense and shifted to higher wave numbers, demonstrating the possibility of His-PPy and Cr(VI) ions interaction (Xu et al., 2019). The XRD patterns for PPy and His-PPy are displayed in in Fig. 1B (a) and (b) respectively. A broad characteristic peak at $2\theta = 25.4°$ is consistent with amorphous PPy attributed to the π-π interaction of the PPy chains (Amalraj et al., 2016a; Ballav et al., 2012; Kera et al., 2016; Xiang et al., 2021). Notably after PPy modification with histidine amino acid this peak shifted to $2\theta = 22.7°$. Such a shift to lower 2θ values could be explained by an increased spacing of PPy and amorphous nature of the macromolecular chains in the His-PPy which are favourable for adsorption of ions (Kera et al., 2016).

The SEM and TEM images of the His-PPy nanocomposite are shown in Fig. 2a and b. These micrographs depict semi-spherical to spherical agglomerated structures of size 200 to 500 nm. Similar observations were obtained using PPy-glycine, PPy-threonine and PPy-aspartic acid doped structures (Amalraj et al., 2016a and b, Ballav et al., 2012).

The EDX spectra for His-PPy before and after Cr(VI) removal displayed in Fig. 3A comprises of bands at 0.27, 0.39, 0.53 and 2.33 keV attributed to C, N, O and S respectively. Additionally, in the spectrum, two additional peaks at binding energies of 5.4 and 5.9 keV, shown in Fig. 3A(b) induced by Cr thus confirming Cr(VI) ions adsorption onto His-PPy (Amalraj et al., 2016b, Cheng et al., 2021, Kera et al., 2018). The XPS survey spectra for His-PPy before and after Cr(VI) removal exposed in Fig. 3B contains peaks attributed to C 1 s, Cl 2p, Cl 2 s, N 1 s and O 1 s at 284, 197, 232, 400 and 533 eV respectively (Ballav et al., 2012; Chigondo et al., 2019; Kera et al., 2018; Wei et al., 2020). Furthermore, the Cr 2p peaks are observed in Fig. 3B(b) which can be split

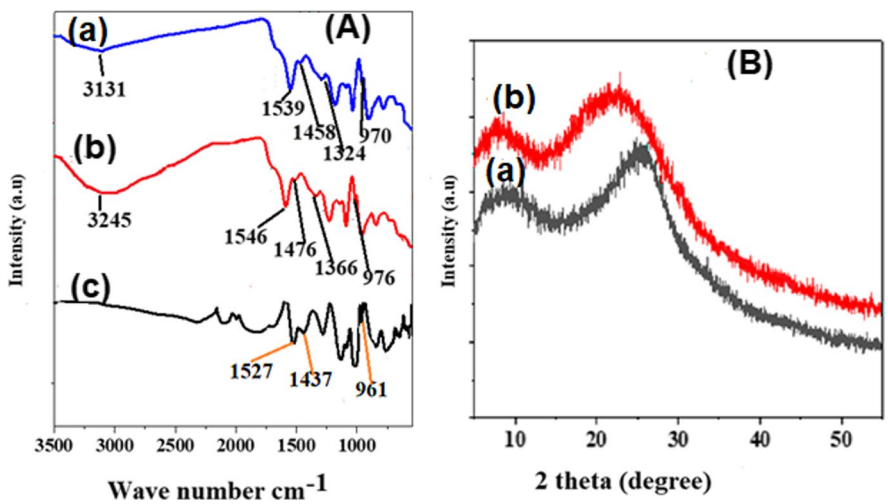

Fig. 1 **A** (a) FTIR spectra of His-PPy nanocomposite (a) before (b) after Cr(VI) ions removal and (c) pristine PPy. **B** XRD patterns of (a) pristine PPy (b) His-PPy nanocomposite

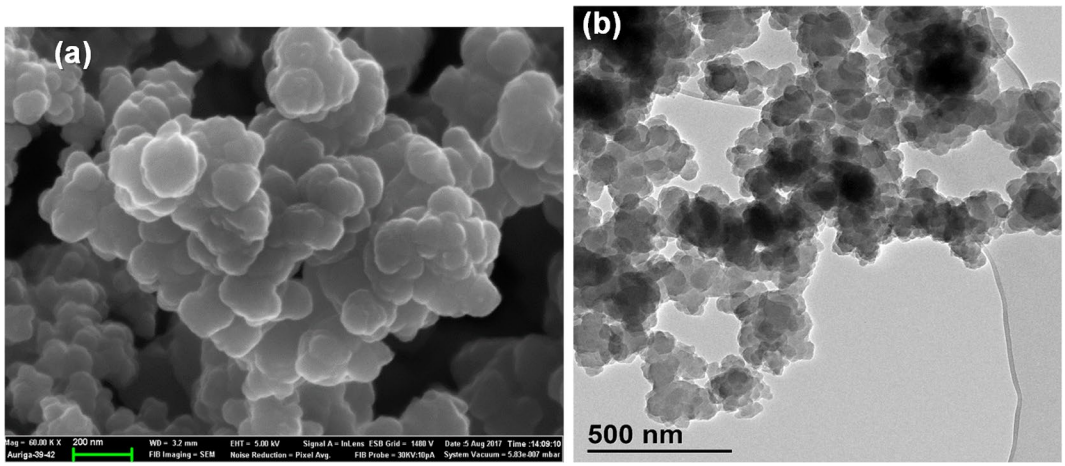

Fig. 2 **a** FE-SEM and (**b**) TEM images His-PPy nanocomposite

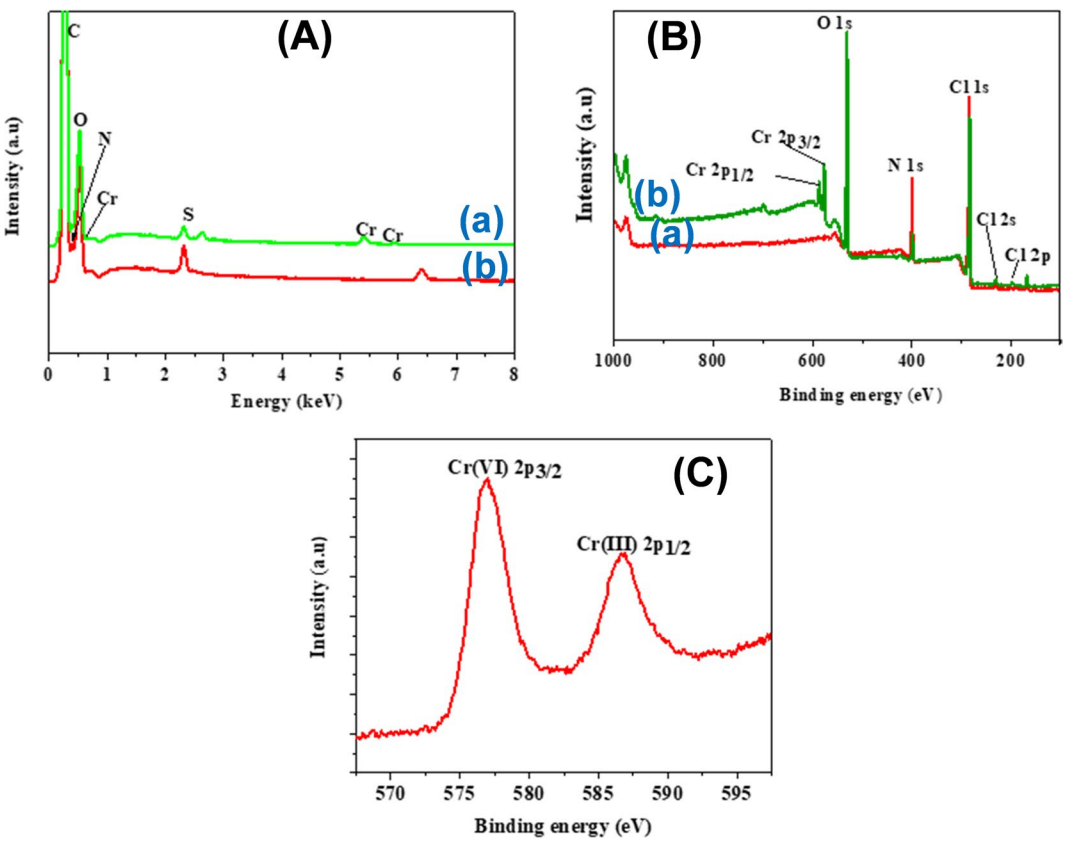

Fig. 3 **A** EDX spectra of His-PPy nanocomposite (a) before and (b) after Cr (VI) adsorption. (**B**) Wide-scan XPS spectra of His-PPy nanocomposite (a) before and (b) after Cr(VI) ions adsorption. **C** Cr 2p XPS spectrum of His-PPy nanocomposite

into binding energies of 577 and 586 eV depicted in Fig. 3C. These match Cr ($2p_{3/2}$) and Cr ($2p_{1/2}$) binding energies confirming of Cr(VI) ions adsorption and reduction to Cr(III) (Amalraj et al., 2016a, Ballav et al., 2012, Chen et al., 2021, Fang et al., 2018). The ratios of the N and O-peaks in XPS change after adsorption of Cr(VI) ion because the N atoms of the nanocomposite moiety take part in the adsorption process through oxidation and reduction (Li et al., 2020). The doping histidine increases the adsorption sites ($-NH^{3+}$ and $-COOH$) and reduction sites ($-N-N-$) of His-PPy. These adsorption and reduction sites form multilayer adsorption by electrostatic adsorption and ion exchange to enrich more Cr(VI)(Li et al., 2020).

3.2 Optimisation of Adsorption

Adsorption studies were conducted to determine the optimum synthesised adsorbent with 1.1, 1.2 and 1.3 g of histidine doped PPy. It was found that the nanocomposite produced from 1.3 g histidine mixture with PPy produced the highest adsorption efficiency for 200 mg L^{-1} of Cr(VI) ions using 0.05 g of adsorbent at pH 2. Accordingly, it was adopted for the rest of the adsorption studies.

3.3 Effect of pH on the Removal of Cr(VI) Ions

During the adsorption process, solution pH is important as it affects Cr(VI) ions speciation, surface chemistry of the adsorbent and the extent of functional groups protonation (Yang et al., 2022). Figure 4a depicts the effect of pH on the percentage Cr(VI) ions removal. The highest removal efficiency (99.1%) was observed at pH 2 with the removal efficiency rapidly declining with increase in pH attaining 12.1% at pH 12. This shows that Cr(VI) ions adsorption is favoured by low pH. Cr(VI) exists as H_2CrO_4 at pH less than 1, $HCrO_4^-$ and $Cr_2O_7^{2-}$ at pH $2-6$, $Cr_2O_7^{2-}$ and CrO_4^{2-} at pH $6-8$ and CrO_4^{2-} at pH more than 8 (Adeiga et al., 2022, Dinker et al., 2015, Dutta et al., 2021, Nguyen et al., 2019). Thus, its removal at low pH is predominantly due to electrostatic attractions between positively charged nitrogen atoms of amino groups in the His-PPy moiety and the predominantly negative Cr(VI) species (Wang et al., 2022). Furthermore, the reaction in Eq. (4) is likely to take place at low pH due to the presence of electron rich polymer matrix resulting in Cr(VI) ions drastically diminishing (Chigondo et al., 2019):

$$CrO_4^{2-} + 7H^+ \leftrightarrow 3Cr^{3+} + 4H_2O \quad (4)$$

On the other hand, as the pH increases the predominant species CrO_4^{2-} competes with hydroxyl ions for adsorption. The pH at point-of-zero charge (pH_{pzc}) of the His-PPy was determined to be 7.70 as displayed in Fig. 4b. Below this pH the adsorbent surface is positively charged while above pH_{pzc} it becomes negatively charged. This further supports the previous hypothesis of electrostatic attractions being predominant below pH_{pzc} and protonation becoming less significant above the pH_{pzc} as OH^- ions dominate the environment hence repulsion between the surface and negatively charged Cr(VI) ions (Du et al., 2020; Dutta et al., 2021),

3.4 Effect of Adsorbent Dose

The effect of adsorbent dose on the removal of of 200 mg L^{-1} Cr(VI) ions was studied by varying the amounts of the adsorbent from 0.01 to 0.07 g at pH 2. Figure 4c shows that there is an increase in percenatge Cr(VI) ions removal from 64.1 to 99.0% as the adsorbent dose increased from 0.01 to 0.05 g. This increase could be ascribed to an increase in available adsorbent active sites and increase in adsorbent-adsorbate collisions (Du et al., 2020, Katata-Serua et al., 2020). Furthermore, as the adsorbent dosage increases beyond 0.05 g the percentage removal becomes almost constant attributed to the overlap of active sites at high dosage as well as equilibration between Cr(VI) ions in solution and ions on the adsorbent (Fan et al., 2017, Katata-Seru et al., 2020).

3.5 Adsorption Isotherms

Adsorption isotherm models can be established by studying the effect of temperature which will culminate in the evaluation of the adsorption capacity of the adsorbent as well as establishing the thermodynamic parameters of adsorption process. In this study this was accomplished through the variation of temperature from 15 to 45 °C at pH 2 using 50 mL of 50–500 mg $L.^{-1}$ Cr(VI) ions solutions and 0.05 g adsorbent dose for contact time of 24 h. The results are revealed in Fig. 5a. The adsorption of Cr(VI) ions onto His-PPy

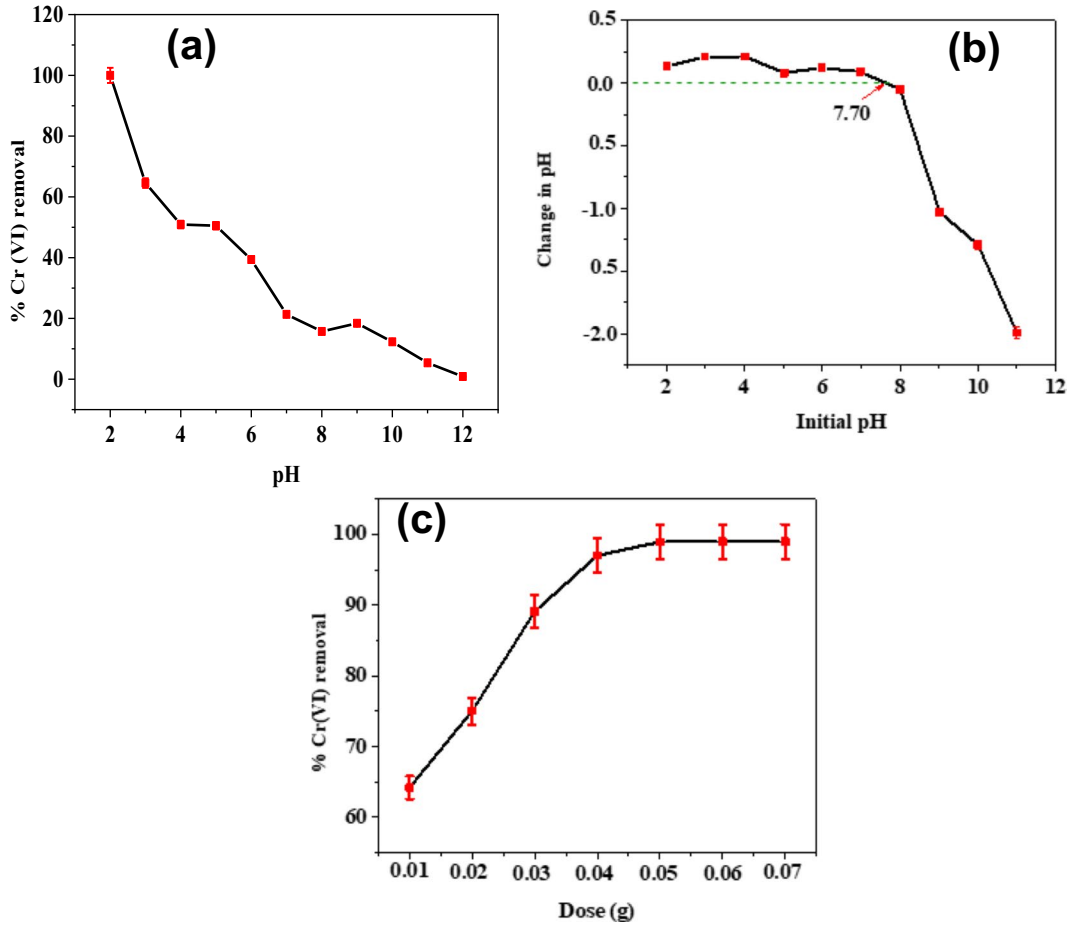

Fig. 4 **a** Effect of pH on the % Cr(VI) removal using 200 mg L^{-1} Cr(VI) ions solution (adsorbent dose: 0.05 g/50 mL of Cr(VI) ions solution contact time: 24 h and temperature: 25 °C (**b**) Determination of pH at point-of-zero charge of His-PPy. **C** Effect of adsorbent dose on adsorption of Cr(VI) ions onto His-PPy using 200 mg L^{-1} Cr(VI) ions solution at pH 2 and 25 °C

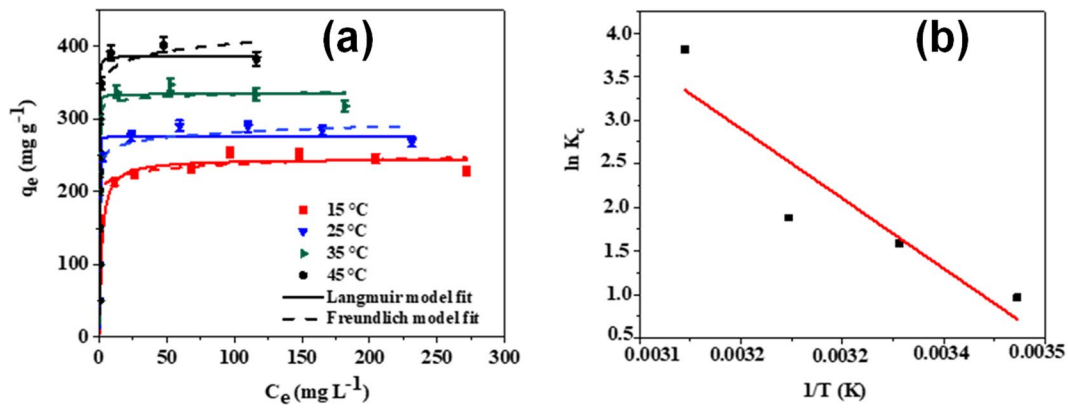

Fig. 5 Adsorption equilibrium isotherms for Cr(VI) ions removal onto His-PPy and fit of data to (**a**) nonlinear Langmuir and Freundlich models. **b** Van't Hoff's plot

increased with increase in temperature, suggesting the endothermic nature of the adsorption. An investigation into heterogeneity and homogeneity of adsorbate on adsorbent surface was achieved through the application of the Langmuir and Freundlich isotherms (Islam et al., 2019). The Langmuir linear and nonlinear isotherms are represented by Eqs. (5) and (6) (Foo and Hammed, 2010, Tan et al., 2017)

$$\frac{C_e}{q_{\ e}} = \frac{1}{q_m b} + \frac{C_e}{q_m} \tag{5}$$

$$q_e = \frac{bq_{mC_e}}{1 + bC_e} \tag{6}$$

where C_e (mg L^{-1}) and q_e (mg g^{-1}) are the equilibrium concentration of Cr(VI) ions and the quantity adsorbed per unit mass of adsorbent respectively. q_m and b (L mg^{-1}) represent the maximum adsorption capacity and the Langmuir constant related to the affinity for the binding sites for Cr(VI) ions respectively (Tan et al., 2017).

The dimensionless separation factor (R_L) in Eq. (7) stipulates the favourability or non-favourability of the adsorption process.

$$R_L = \frac{1}{1 + bC_o} \tag{7}$$

where R_L values from 0 to 1 for each of the different initial Cr(VI) ions concentration propose favourable adsorption. Nonetheless $R_L = 0$ $R_L = 1$ and $R_L > 1$ suggest linear irreversible and unfavourable process respectively (Tan et al., 2017, Xiang et al., 2021). In this study R_L values ranged between 0.00023 and 0.00161 (Table 1) an indication of a favourable adsorption process at all temperatures studied (Chen et al., 2021).

The nonlinear and linear Freundlich isotherm models represented by Eqs. (8) and (9) (Foo and Hammed, 2010, Tan et al., 2017) were used to evaluate the adsorption behaviour of the His-PPy adsorbent towards Cr(VI) ions.

$$q_e = K_f C_e^{\ 1/n} \tag{8}$$

$$lnq_e = lnK_f + \frac{1}{n} lnC_e \tag{9}$$

Table 1 Langmuir and Freundlich parameters for the adsorption of Cr(VI) ions onto His-PPy

Isotherm model	Temperature (°C)			
	15	25	35	45
Langmuir Linear				
q_m (mg g^{-1})	236.00	274.73	322.58	386.10
b (L m g^{-1})	1.24	1.24	2.07	8.67
R_L	0.00161	0.00161	0.000965	0.00023
R^2	0.9970	0.9990	0.9992	0.9997
Freundlich Linear				
K_f (mg g^{-1})	185.84	47.21	52.88	59.09
1/n	0.058	0.0418	0.022	0.053
R^2	0.806	0.950	0.707	0.922

The Freundlich constants K_f (mg g^{-1}) and *1/n* are associated with the adsorption capacity and intensity of adsorption respectively (Tan et al., 2017). The values of *1/n* are typically between 0 and 1. Nevertheless, a value is closer to zero means more surface heterogeneity. In this study 1/*n* values ranged from 0.0224 to 0.0581 within the temperature range of 15 to 45 °C (Table 1) suggesting surface heterogeneity (Tan et al., 2017, Wang et al., 2018).

The Langmuir isotherm data displayed in Table 1 show that (R^2_{linear}=0.997–0.999) are higher than those for the Freundlich isotherm (R^2_{linear}=0.707–0.940) at any specified temperature. Consequently, the Langmuir model articulates the adsorption better, indicating monolayer coverage throughout adsorption of Cr(VI) ions Foo and Hammed, 2010, Kera et al., 2018, Tan et al., 2017). The evaluated Langmuir maximum adsorption capacities, q_{max} values were 236.00, 274.73, 322.58 and 386.10 mg g^{-1} at 15, 25, 35 and 45 °C respectively indicative of an increase in adsorption capacity with temperature. Cognate observations were obtained by Amalraj et al., (2016a and b), Ballav et al. (2012) with PPy-glycine PPy-threonine doped and PPy-aspartic acid adsorbents, respectively.

A comparison of the adsorption capacity of the His-PPy adsorbent with adsorbents of the same nature from previous studies is displayed in Table 2. The adsorption efficiency of the His-PPy nanocomposite fairs well and thus has the potential for utilisation in the removal of Cr (VI) ion removal from water.

Table 2 Comparative evaluation of Cr(VI) ions adsorption capacity of His-PPy with other reported materials

Adsorbent	Langmuir adsorption capacity q_{max} (mg g^{-1})	Temperature (°C)	pH	Concentration (mg L^{-1})	References
Fe_3O_4@PPyArg	322.58	25	2.0	200	(Chigondo et al., 2019)
PPy–mPD	183.20	25	2.0	200	(Kera et al., 2018)
Magnetic UiO-66@Ppy	259.1	25	2.0	200	(Du et al., 2020)
CAL-PPy	66.14	45	2.0	200	(Yang et al., 2022)
PPy-Sugarscane bagasse	251.0	25	2.0	200	(Chen et al., 2020)
GCS@PPy/L-cys	209.18	-	2.0	100	(Li et al., 2020)
Threonine/PPy	185.50	25	2.0	200	(Amalraj et al., 2016b)
Asp/PPy	176.67	30	2.0	200	(Amalraj et al., 2016a)
PPy—Fe_3O_4 – SW	144.93	30	2.0	50	(Sarojini et al., 2021)
His-PPy	274.73	25	2.0	200	(This study)

3.6 Thermodynamic Parameters for Cr(VI) Ions Adsorption Onto His-PPy

Evaluated thermodynamic parameters such as change in Gibbs free energy ($\Delta G°$), enthalpy change ($\Delta H°$) and entropy change ($\Delta S°$) can be used to explain the nature of the adsorption process and its likelihood. These were evaluated using Eqs. (10)-(12) (Papita & Chowdhury, 2011):

$$\Delta G° = -RTlnK_c = -RTln\left(m\frac{q_e}{C_e}\right) \tag{10}$$

$$K_c = \left(m\frac{q_e}{C_e}\right) \tag{11}$$

$$ln\left(m\frac{q_e}{C_e}\right) = \frac{\Delta S°}{R} - \frac{\Delta H°}{RT} \tag{12}$$

where R (J mol^{-1} K^{-1}), T (K), m (g/L) and K_c (dimensionless by considering the activity coefficient of the adsorbate as 1 mol/L) are the molar gas constant, temperature, adsorbent dose and equilibrium constant, respectively (González-López et al., 2022, Kera et al., 2018). The values of $\Delta H°$ and $\Delta S°$ were obtained from the slope and intercept of a plot of $ln\ K_c$ against $1/T$ as revealed in Fig. 5b respectively. Table 3 displays the subsequent thermodynamic data obtained from this plot. It was determined that enthalpy change ($\Delta H°$) had a magnitude of + 66.64 kJ mol^{-1} whilst Gibbs free energy ($\Delta G°$) change ranged from –2.308 to –10.079 kJ mol^{-1} signifying an endothermic and chemisorption nature of the process (Papita & Chowdhury, 2011; Shang et al., 2018). The decrease in magnitude of ($\Delta G°$) with temperature can be explained by dispersion forces decrease with increasing of the experimental temperature from 15 to 45 °C could be due to an increase in the kinetic energy of the molecules associated with the increased rate of the motion of particles within the pore space can leading to a decrease of the interaction forces. Similar results were observed by Fulazzaky (2019).

Table 3 Thermodynamic parameters data for Cr(VI) ions adsorption onto His-PPy

Temperature (°C)	$\Delta G°$ (kJ mol^{-1})	$\Delta H°$ (kJ mol^{-1})	$\Delta S°$ (kJ mol^{-1} K^{-1})
15	-2.308	+ 66.64	+ 237.67
25	-3.923		
35	-4.820		
45	-10.079		

There was an increase in feasibility of the adsorption process with increasing temperature within the range 15–45 °C. Furthermore, a positive value of the entropy change ($\Delta S°$) (+ 237.67 kJ mol^{-1} K^{-1}) indicates increase in randomness at the solid–liquid interface attributed to structural modifications in adsorbate and adsorbent as well as affinity between the two (Kera et al., 2017; Papita & Chowdhury, 2011).

3.7 Adsorption Kinetics

Adsorption kinetics for Cr(VI) ions removal using His-PPy nanocomposite was investigated. The effect of contact time on the adsorption of Cr(VI) ions at 50, 100 and 150 mg L^{-1} initial concentrations of Cr(VI) ions is exposed in Fig. 6a. It can be observed that initially adsorption capacity of Cr(VI) increases rapidly as contact time increases with the equilibrium times of 60, 120 and 150 min respectively. This is attributed to the availability of a large number of vacant adsorption sites on the surface of the His-PPy nanocomposite (Dutta et al., 2021; Fang et al., 2018). However with prolonged contact time the Cr(VI) ions removal rate diminished sharply as the Cr(VI) ions concentration and active adsorption sites decreased (Li et al., 2020).

The pseudo-first-order and pseudo-second-order adsorption models are commonly applied to describe the adsorption process. In that respect the kinetics of the adsorption data in this study was fitted to linear and nonlinear pseudo-first-order and pseudo-second-order kinetic models which are represented by Eqs. (13)-(16) (Tan et al., 2017):

$$q_t = q_e\left(1 - exp^{-k_1 t}\right) \tag{13}$$

$$log\left(q_e - q_t\right) = log\left(q_e\right) - \frac{k_1}{2.303}t \tag{14}$$

$$q_t = \frac{k_2 {q_e}^2 t}{1 + k_2 q_e t} \tag{15}$$

$$\frac{t}{q_t} = \frac{1}{k_2 {q_e}^2} + \frac{t}{q_e} \tag{16}$$

where k_1 (min^{-1}) and k_2 (g/m $g^{-1}.min^{-1}$) are the pseudo-first-order and pseudo-second-order-rate constants respectively. q_e and q_t (mg g^{-1}) are the adsorption capacities at equilibrium and time t (min) respectively. The data for pseudo-first-order and pseudo-second-order linear kinetics are shown Table 4. The coefficient values R^2 for the determination of the pseudo-second-order linear ($R^2 = 0.999–1.000$ are higher than those for pseudo-first-order ($R^2 = 0.948–0.975$). Thus, the Cr(VI) ions adsorption onto the His-PPy adsorbent could be better described by the pseudo-second-order kinetic model depicting a dependence on mass transfer particle diffusion and physicochemical interaction between Cr(VI) ions and His-PPy in aqueous solution (Karthikeyan et al., 2021). Furthermore, it means rate-limiting step is chemical sorption or chemisorption and the adsorption rate is dependent on adsorption capacity not on concentration of adsorbate (Tan et al., 2017).

Furthermore, to understand the rate controlling step in Cr(VI) ions adsorption onto His-PPy the Weber and Morris intraparticle diffusion model was

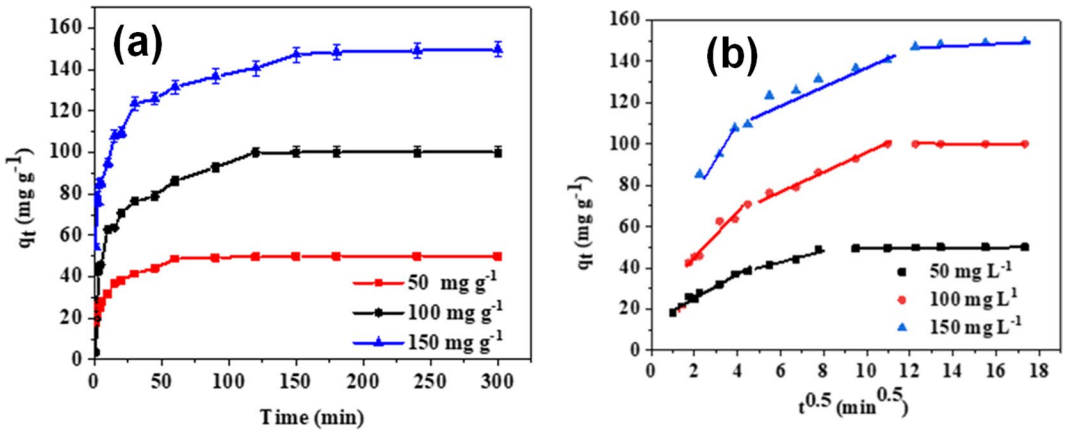

Fig. 6 **a** effect of contact time on the adsorption of Cr(VI) ions onto His-PPy (pH = 2 adsorbent dose 0.05 g/50 mL of Cr(VI) ions and temperature 25 °C). **b** Intra-particle diffusion model for the Cr(VI) ions adsorption onto His-PPy nanocomposite

Table 4 Kinetics parameters for the sorption of Cr(VI) ions adsorption onto His-PPy nanocomposite at different concentrations

Kinetic models	Initial concentration (mg L^{-1})		
	50	100	150
Pseudo-first-order Linear			
k_1 (min^{-1})	4.9×10^{-2}	2.56×10^{-2}	2.09×10^{-2}
q_e (mg g^{-1})	49.31	99.95	147.17
R^2	0.975	0.948	0.971
Pseudo-second-order Linear			
k_2 (g $m^{-1}.min^{-1}$)	4.56×10^{-3}	9.40×10^{-3}	1.18×10^{-3}
q_e (mg g^{-1})	49.31	99.95	147.17
R^2	1.000	1.000	0.999
Intra-particle diffusion model parameters			
	Cr (VI) ions concentration (mg L^{-1})		
	50	100	150
k_{int} (mg $g^{-1}.min^{-0.5}$)	6.400	14.407	15.450
C_i (mg g^{-1})	13.035	26.494	49.182

applied. The Webber-Morris model (Tan et al., 2017) is expressed by Eq. (17):

$$q_t = k_{int}t^{0.5} + C_i \quad (17)$$

where k_{int} (mg g^{-1} $min^{-0.5}$) and C_i (mg g^{-1}) are the intra-particle diffusion rate constant and a constant associated with the magnitude of the boundary layer thickness respectively. From Fig. 6b it is revealed that the plots of $t^{0.5}$ against q_t for different initial concentrations of Cr(VI) ions solutions comprises three stages. Consequently the adsorption of Cr(VI) ions was a three staged process which involved the faster film diffusion followed by slower adsorption due to intra-particle diffusion with the third region depicting the final equilibration stage attributed to decreased Cr(VI) ions concentration (Adeiga et al., 2022, Fang et al., 2018, Li et al., 2020). Furthermore, the high magnitude of boundary layer thickness C_i (13.035–49.182 confirms the significance of surface diffusion on the rate limiting step (Bhaumik et al., 2016).

3.8 Effect of Co-existing Ions

A wide range of industrial activities such as mining, electroplating and metal purification produce wastewater with high levels of Cr(VI) as well as other dissolved anions and cations which may interfere with the adsorption of a targeted pollutant. Figure 7. shows the effect of Cl^-, SO_4^{2-}, NO_3^-, HCO_3^-, PO_4^{3-}, Zn^{2+}, Cu^{2+}, Ni^{2+}, Mg^{2+}, Ca^{2+} and multi-ions at 0, 50, 100 and 150 mg L^{-1} on Cr (VI) ions adsorption onto the His-PPy nanocomposite. As observed in Fig. 7, Zn^{2+}, Cu^{2+}, Ni^{2+}, Mg^{2+} and Ca^{2+} cations did not interfere with Cr(VI) ions removal at due to repulsion by the positively charged His-PPy surface. Furthermore, the Cl^-, SO_4^{2-}, NO_3^- and PO_4^{3-} anions had negligible effects on the removal of Cr(VI) ions demonstrating high selectivity of the adsorbent. Cl^- and NO_3^- ions are low-affinity ligands which form weak outer sphere complexes with binding sites (Liang et al., 2017). On the other hand PO_4^{3-} ions may not

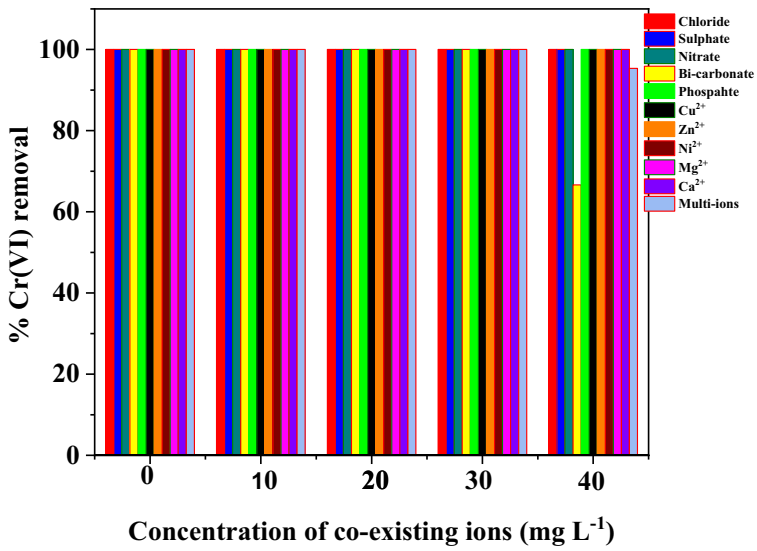

Fig. 7 Effect of co-existing ions on Cr(VI) ions adsorption at pH 2 (adsorbent dose: 0.05 g/50 mL of Cr(VI) ions solution contact time: 24 h and temperature: 25 °C)

bind on the adsorption sites as Cr(VI) ions hence no effect (Kera et al., 2018). SO_4^{2-} ions's lack of interference with Cr(VI) ions adsorption at pH 2 could be attributed to higher enthalpy of hydration (−1080 $kJmol^{-1}$) relative to $HCrO_4^-$ (−184 kJ mol^{-1}) and CrO_4^{2-} (−950 kJ mol^{-1}) (Ballav et al., 2014). Moreover, the high selectivity of His-PPy for Cr(VI) can be also be attributed to the high positive redox potential of $HCrO_4^-$ anions the major form in which Cr(VI) exists in solutions at low pH (Kera et al., 2018). This makes them to be easily reduced to Cr(III) by the PPy moiety. The Cl^-, SO_4^{2-}, NO_3^- and PO_4^{3-} anions are weaker oxidising agents than $HCrO_4^-$ ions hence they do not lower the removal efficiency. Only at very high concentration (40 mg L^{-1}), do HCO_3^- ions reduce Cr(VI) ions uptake to 67.2% but at low concentration this is insignificant. Multi-ions also have an effect on the removal of C(VI) ions at 40 mg/L.This could be attributed to more generation of OH^- during hydrolysis of HCO_3^- at low pH and very high concentrations which competitively are adsorbed on the His-PPy nanocomposite with Cr(VI) ions (Preethi et al., 2017).

3.9 Performance on Industrial Wastewater Samples

The as-prepared His-PPy was evaluated for suitability to selective adsorption of Cr(VI) ions from chromium ores leaching effluent samples obtained from Gweru heavy industrial area wastewater in the Midlands Province of Zimbabwe. The initial concentration of Cr(VI) in the effluent was 120 mg L^{-1} and at pH 0.8. The pH of the effluent was adjusted to 2, the His-PPy nanocomposite optimal pH for Cr(VI) ions removal followed by addition of 0.01 to 0.07 g adsorbent dosages to 50 mL industrial samples agitated for 24 h at 25 °C. From Fig. 8A it can be observed that the Cr(VI) ions were completely removed at adsorbent dosage above 0.04 g showing that the His-PPy nanocomposite has the potential to remove the Cr(VI) ions from waste water.

3.10 Desorption Studies

The recyclability of an adsorbent is an important criterion for the evaluation of its potential practicality. The adsorbed Cr(III) emanating from Cr (VI) reduction by the electron-rich polypyrrole moieties, was desorbed with HCl for the adsorption cycle tests. Figure 8B exhibits the adsorption capacity of His-PPy in each treatment cycle. The results illustrate that the adsorption capacity remained largely constant up to three cycles but declined to 65% in 4th cycle. The reduction in adsorption capacity might be attributed to the presence Cr(III) ions occupying portions of the active sites and polymer chain rupture as a result of recurrent adsorption–desorption of Cr(VI) ions (Kera et al., 2018; Xiang et al., 2021). As a result, His-PPy could be recycled for three successive cycles retaining its adsorption capacity to demonstrate good reusability of the nanocomposites.

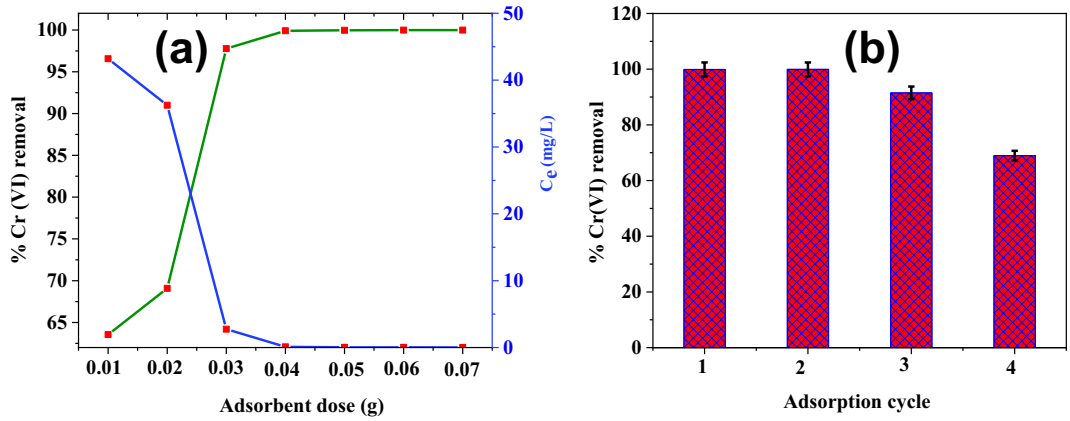

Fig. 8 **a** Effect of His-PPy dose on % Cr(VI) ions removal and equilibrium concentration in wastewater samples. **b** Adsorption and desorption cycles for the His-PPy nanocomposite, adsorbent dose: 0.05 g/50 mL of Cr(VI) ions solution contact time: 24 h and temperature: 25 °C)

3.11 Adsorption Mechanism

The probable mechanisms for Cr(VI) ions adsorption onto His-PPy are ion exchange, electrostatic attractions, reduction and hard base (amino substituents)-hard acid ((Cr(III)) chelation (Chen et al., 2020, Chigondo et al., 2019, Sarojini et al., 2021, Sun et al., 2020). At pH 2–6 Cr(VI) ions exist predominantly as $Cr_2O_7^{2-}$ and $HCrO_4^-$ species. The pH_{pzc} of His-PPy was estimated to be 7.7 as illustrated in (Fig. 4A). At $pH < pH_{pzc}$ the nanocomposite is positively charged and protonated so the polar nitrogen species (N^+) which become active sites for $Cr_2O_7^{2-}$ or $HCrO_4^-$ adsorption by electrostatic attractions as illustrated in Eqs. (18) and (19) (Nguyen et al., 2019).

$$-NH_2^+ + HCrO_4^- \rightarrow -NH_2^+ - - - NCrO_4^- \quad (18)$$

$$-NH_2^+ + HCrO_4^- \rightarrow -NH_2^+ - - - NCrO_4^- \quad (19)$$

From Fig. 1A(b) and (c) the FTIR spectra of His-PPy exhibited a band shift at 3131 cm^{-1} consistent with the NH stretching vibration to 3282 cm^{-1} after Cr(VI) adsorption. This is attributable to the interactions between Cr(VI) ions and positively charged nitrogen containing fragments of PPy and histidine at low pH. Furthermore, based on our previous studies (Chigondo et al., 2019) the positive $–NH^+$ group in a polymer moiety has the capability to reduce $Cr_2O_7^{2-}$ and $HCrO_4^-$ to Cr(III) due to inter-changeable states PPy^0 and PPy^+ under an acidic milieu (Sun et al., 2020) as shown Eqs. (20)-(22) (Fang et al., 2018, Sun et al., 2020).

$$PPy^+ + e^- \rightarrow PPy^0 \quad (20)$$

$$3PPy^0 + 7H^+ + HCrO_4^- \rightarrow Cr^{3+} + 4H_2O + 3PPy^+ \quad (21)$$

$$3PPy^0 + Cr_2O_7^{2-} + 14H^+ 6e^- \rightarrow Cr^{3+} + 3PPy^+ + 4H_2O \quad (22)$$

Additionally Cr(III) ions can form dative bonds with the nitrogen atoms of the histidine dopant which resulting in strong acid–base interactions (Chen et al., 2020, Fang et al., 2018; Zhao et al., 2016; Li et al., 2020) as illustrated in Eq. (23).

$$-N^+ + Cr^{3+} \rightarrow -N^+ : \rightarrow Cr^{3+} \quad (23)$$

The XPS comprehensively validates the adsorption mechanisms. The XPS Cr 2p core level spectra are typically from 575.0–580.0 eV (Cr $2p_{3/2}$) and 585.0–588.0 eV (Cr $2p_{1/2}$) for Cr(III) while Cr(VI) species exhibit values in the range 580.0–580.5 eV (Cr $2p_{3/2}$) and 589.0–590.0 eV (Cr $2p_{1/2}$) (Fang et al., 2018; Goddeti et al., 2020; Zhang et al., 2020). In this study the binding energy of Cr $2p_{3/2}$ and Cr $2p_{1/2}$ were detected at 577.4 and 586.5 eV respectively (Fig. 3B(b)) characteristic of Cr(III) (Bhaumik et al., 2016; Zhang et al., 2020). Such values suggest the presence of both Cr(VI) and Cr(III) species on adsorbent surface.

4 Conclusion

The synthesis and characterisation of a novel His-PPy nanocomposite was successfully accomplished and applied for the removal of Cr(VI) ions from aqueous solution. Consequently, not only abundant reduction-adsorption sites were increased but also effective prevention of oxidative breakdown of the nanocomposite surface structure. Further, evaluation of adsorption studies demonstrated that the His-PPy nanocomposite adsorbent was highly efficient in removing extremely noxious Cr(VI) ions with a Langmuir maximum adsorption capacities of 236.00, 274.73, 322.58 and 386.00 mg g^{-1} at 25 to 45 °C respectively at pH 2 and adsorbent of dosage of 1000 mg/L. The reduction-adsorption capability of the His-PPy nanocomposite was remarkably improved by doping with L-histidine with three treatment cycles without any loss of adsorption capacity. Moreover, it was found out that the thermodynamic data demonstrated chemisorption, spontaneous and endothermic nature of adsorption. Based on FTIR and XPS data, the mechanisms of adsorption were hypothesised to be mainly electrostatic attractions, reduction and chelation. Thus, the His-PPy nanocomposite has the potential for detoxification of hexavalent chromium polluted water.

Acknowledgements The authors acknowledge the assistance rendered by Manicaland State University of Applied Sciences and Midlands State University. The characterisation facility at the DST-CSIR National Centre for Nanostructured Materials Pretoria South Africa is acknowledged for assisting with the materials characterization.

Author Contributions Conceptualization Methodology Software (Marko Chigondo), Data curation, writing original

draft preparation (Fidelis Chigondo, Maposa Munashe and Marko Chigondo), Visualization and Investigation (Marko Chigondo, Fidelis Chigondo and Benias Nyamunda), Supervision. (Marko Chigondo, Fidelis Chigondo and Benias Nyamunda), Writing- Reviewing and Editing (Marko Chigondo, Benias Nyamunda, Munashe Maposa, Knowledge Nyenyayi, Delroy Nyadenga).

Funding This work was supported by the Department of Chemical and Processing Engineering Manicaland State University of Applied Sciences Zimbabwe and Department of Chemical Sciences Midlands State University Zimbabwe.

Data Availability No datasets were generated or analysed during the current study.

Declarations

Ethics Approval Not applicable.

Consent to Participate Yes.

Consent to Publish Yes.

Competing Interests The authors have no relevant financial or non-financial interests to disclose.

References

Adeiga, O., Velempini, T., & Pillay, K. (2022). Polyaniline-decorated Macadamia nutshell composite: an adsorbent for the removal of highly toxic Cr(VI) and efficient catalytic activity of the spent adsorbent for reuse. *Polymer Bulletin*, 1–23. https://doi.org/10.1007/s00289-021-04009-w

Amalraj, A., Selvi, M. K., Rajeswari, A., & Pius, A. (2016a). Preparation and characterization of aspartic acid doped polypyrrole for the efficient removal of Cr(VI) from aqueous solution. *Journal of Water Process Engineering, 11*, 162–173. https://doi.org/10.1016/j.jwpe.2016.05.005

Amalraj, A., Selvi, M. K., Rajeswari, A., Christy, E. J. S., & Pius, A. (2016b). Efficient removal of toxic hexavalent chromium from aqueous solution using threonine doped polypyrrole nanocomposite. *Journal of Water Processing Engineering, 13*, 88–99. https://doi.org/10.1016/j.jwpe.2016.08.013

Ates, M., Karazehir, T., & Sezai, S. A. (2012). Conducting polymers and their applications. *Current Physical Chemistry, 2*, 224–240. https://doi.org/10.4028/www.scientific.net/MSF.42.207

Baig, U., Rao, R. A. K., Khan, A. A., Sanagi, M. M., & Gondal, M. A. (2015). Removal of carcinogenic hexavalent chromium from aqueous solutions using newly synthesized and characterized polypyrrole-titanium (IV) phosphate nanocomposite. *Chemical Engineering Journal, 280*, 494–504. https://doi.org/10.1016/j.cej.2015.06.031

Ballav, N., Maity, A., & Mishra, S. B. (2012). High efficient removal of chromium (VI) using glycine doped polypyrrole adsorbent from aqueous solution. *Chemical Engineering Journal, 198*, 536–546. https://doi.org/10.1016/j.cej.2012.05.110

Ballav, N., Choi, H. J., Mishra, S. B., & Maity, A. (2014). Synthesis characterization of Fe_3O_4@ glycine doped polypyrrole magnetic nanocomposites and their potential performance to remove toxic Cr (VI). *Journal Ind Engineering Chemistry, 20*, 4085–4093. https://doi.org/10.1016/j.jiec.2014.01.007

Bhaumik, M., Maity, A., Srvivasu, V. V., & Onyango, M. M. (2011). Enhanced removal of Cr (VI) from aqueous solution using polypyrrole/Fe_3O_4 magnetic nanocomposite. *Journal of Hazardous Materials, 190*, 381–390.

Bhaumik, M., Maity, A., Srinivasu, V. V., & Onyango, M. S. (2012). Removal of hexavalent chromium from aqueous solution using polypyrrole-polyaniline nanofibers. *Chemical Engineering Journal, 181*, 323–333. https://doi.org/10.1016/j.cej.2011.11.088

Bhaumik, M., Agarwal, S., Gupta, V. K., & Maity, A. (2016). Enhanced removal of Cr(VI) from aqueous solutions using polypyrrole wrapped oxidized MWCNTs nanocomposites adsorbent. *Journal of Colloid Interface Science, 470*, 257–267. https://doi.org/10.1016/j.jcis.2016.02.054

Chen, J., Liang, Q., Ploychompoo, S., & Luo, H. (2020). Functional rGO aerogel as a potential adsorbent for removing hazardous hexavalent chromium: Adsorption performance and mechanism. *Environmental Science Pollution Research, 27*, 10715–10728. https://doi.org/10.1007/s11356-019-07365-3

Cheng, J., Gao, J., Zhang, J., Yuan, W., Yan, S., Zhou, J., Zhao, J., & Feng, S. (2021). Optimization of hexavalent chromium biosorption by Shewanella putrefaciens using the Box-Behnken design. *Water, Air, & Soil Pollution, 232*, 1–14. https://doi.org/10.1007/s11270-020-04947-7

Chigondo, M., Paumo, H. K., Bhaumik, M., Pillay, K., & Maity, A. (2019). Magnetic arginine functionalized polypyrrole with improved and selective chromium(VI) ions removal from water. *Journal Molecular Liquids, 275*, 778–791. https://doi.org/10.1016/j.molliq.2018.11.032

Das, R., Hugues, K.P., & Maity, A. (2019). Surface-modified conducting polymer-based nanostructured materials for the removal of toxic heavy metals from wastewater. *In Advanced Nanostructured Materials for Environmental Remediation, Springer Cham*, 111–144. https://doi.org/10.1007/978-3-030-04477-0_5

Deng, X., Qi, L., & Zhang, Y. (2018). Experimental study on adsorption of hexavalent chromium with microwave-assisted alkali modified fly ash. *Water, Air, & Soil Pollution, 229*, 1–6. https://doi.org/10.1007/s11270-017-3679-8

Dinker, M. K., & Kulkarni, P. S. (2015). Recent advances in silica-based materials for the removal of hexavalent chromium: a review. *Journal Chemical Engineering Data, 60*, 2521–2540. https://doi.org/10.1021/acs.jced.5b00292

Du, L., Gao, P., Liu, Y., Minami, T., & Yu, C. (2020). Removal of Cr (VI) from aqueous solution by polypyrrole/hollow mesoporous silica particles. *Nanomaterials, 10*, 686. https://doi.org/10.3390/nano10040686

Dutta, S., Srivastava, S. K., & Gupta, A. K. (2021). Polypyrrole-polyaniline copolymer coated green rice husk ash

as an effective adsorbent for the removal of hexavalent chromium from contaminated water. *Material Advance, 2*, 2431–2443. https://doi.org/10.1039/D0MA00862A

Fan, S., Wang, Li, Y., Tang, J., Wang, Z., Tang, J., Li, X., & Hu, K. (2017). Facile synthesis of tea waste/Fe_3O_4 nanoparticle composite for hexavalent chromium removal from aqueous solution. *Royal Society of Chemistry Advances, 7*, 7576–7590.

Fang, W., Jiang, X., Luo, H., & Geng, J. (2018). Synthesis of graphene/SiO_2@ polypyrrole nanocomposites and their application for Cr (VI) removal in aqueous solution. *Chemosphere, 197*, 594–602. https://doi.org/10.1016/j.chemosphere.2017

Foo, K. Y., & Hammed, B. H. (2010). Insights into modelling of isotherm adsorption systems. *Chemical Engineering Journal, 156*, 2–10. https://doi.org/10.1016/j.cej.2009.09.013

Fulazzaky, M. A. (2019). Study of the dispersion and specific interactions affected by chemical functions of the granular activated carbons. *Environmental Nanotechnology, Monitoring & Management, 12*, 100230. https://doi.org/10.1016/j.enmm.2019.100230

Goddeti, S. M. R., Maity, A., & Ray, S. S. (2020). Polypyrrole-coated gum ghatti-grafted poly (acrylamide) composite for the selective removal of hexavalent chromium from waste water. *International Journal of Biological Macromolecules, 164*, 2851–2860. https://doi.org/10.1016/j.ijbiomac.2020.07.324

González-López, M. E., Laureano-Anzaldo, C. M., Pérez-Fonseca, A. A., Arellano, M., & Robledo-Ortíz, J. R. (2022). A critical overview of adsorption models linearization: Methodological and statistical inconsistencies. *Separation & Purification Reviews, 51*, 358–372.

Hsini, A., Naciri, Y., Laabd, M., El Ouardi, M., Ajmal, Z., Lakhmiri, R., & Albourine, A. (2020). Synthesis and characterization of arginine-doped polyaniline/walnut shell hybrid composite with superior clean-up ability for chromium (VI) from aqueous media: Equilibrium reusability and process optimization. *Journal Molecular Liquids, 316*, 113832.

Islam, M. N., Khan, M. N., Mallik, A. K., & Rahman, M. M. (2019). Preparation of bio-inspired trimethoxysilyl group terminated poly(1-vinylimidazole)-modified-chitosancomposite for adsorption of chromium (VI) ions. *Journal of Hazardous Materials, 379*, 120792.

Karthikeyan, P., Elanchezhiyan, S. S., Meenakshi, S., & Park, C. M. (2021). Magnesium ferrite-reinforced polypyrrole hybrids as an effective adsorbent for the removal of toxic ions from aqueous solutions: Preparation characterization and adsorption experiments. *Journal of Hazardous Materials, 408*, 124892. https://doi.org/10.1016/j.jhazmat.2020.124892

Katata-Serua, L. M., Maponya, T. C., Makhado, E., Modibane, K. D., Hato, M. J., Matome, S. M., & Bahadur, I. (2020). Green synthesis of polypyrrole/nanoscale zero valent iron nanocomposite and use as an adsorbent for hexavalent chromium from aqueous solution. *South African Journal of Chemical Engineering, 34*, 1–10. https://doi.org/10.1016/j.sajce.2020.05.004

Kera, N., Bhaumik, M., Ballav, N., Pillay, K., Ray, S. S., & Maity, A. (2016). Selective removal of Cr (VI) from aqueous solution by polypyrrole/2,5-diaminobenzene sulfonic acid composite. *Journal of Colloid Interface Science, 476*, 144–157. https://doi.org/10.1016/j.jcis.2016.05

Kera, N., Bhaumik, B., Kriveshini, K., Ray, S. S., & Maity, A. (2017). Selective removal of toxic Cr (VI) from aqueous solution by adsorption combined with reduction at a magnetic nanocomposite surface. *Journal of Colloids Interface Science, 503*, 214–228. https://doi.org/10.1016/j.jcis.2017.05.018

Kera, N., Bhaumik, B., Kriveshini, K., Ray, S. S., & Maity, A. (2018). m-Phenylenediamine-modified polypyrrole as an efficient adsorbent for removal of highly toxic hexavalent chromium in water. *Materials Today Communication, 15*, 153–164. https://doi.org/10.1016/j.mtcomm.2018.02.033

Li, Y., Peng, L., Guo, J., & Chen, Z. (2020). An Enhanced Reduction-Adsorption Strategy for Cr (VI): Fabrication and Application of l-Cysteine-doped Carbon@ Polypyrrole with a Core/Shell Composite Structure. *Langmuir, 36*, 11508–11516. https://doi.org/10.1021/acs.langmuir.0c01849

Liang, Q., Geng, J., Luo, H., Fang, W., & Yin, Y. (2017). Fast and selective removal of Cr (VI) from aqueous solutions by a novel magnetic Cr (VI) ion-imprinted polymer. *Journal of Molecular Liquids, 248*, 767–774.

Liu, X., Liao, Y., & Gao, H. (2018). Enhancement adsorption of hexavalent chromium from aqueous solution on polypyrrole using ethylamine group. *Journal of Dispersion Science and Technology, 39*, 1394–1402. https://doi.org/10.1080/01932691.2017.1404917

Liu, S., Cao, L., Tian, X., Li, X., Liao, L., & Zhao, C. (2021). Enhanced removal of Cr (VI) using a modified environment-friendly adsorbent. *Water Science and Technology, 83*, 678–688. https://doi.org/10.2166/wst.2021.007

Mahmud, H.N.M.E., Huqa, A.K.O., & binti Yahya, R. (2016). Removal of heavy metal ions from wastewater/aqueous solution by polypyrrole-based adsorbents: a review. *Royal Society of Chemistry Advance*, *6*, 14778-14791, 1–13https://doi.org/10.1039/C5RA24358K

Maity, S., Dubey, A., & Chakraborty, S. (2019). A review on polypyrrole-coated bio-composites for the removal of heavy metal traces from waste water. *Journal of Industrial Textiles*, *51*, 152–173. 1528083719871272 https://doi.org/10.1177/2F1528083719871272

Nguyen, L. H., Nguyen, T. M. P., Van, H. T., Vu, X. H., Ha, T. L. A., Nguyen, T. H. V., Nguyen, X. H., & Nguyen, X. C. (2019). Treatment of hexavalent chromium contaminated wastewater using activated carbon derived from coconut shell loaded by silver nanoparticles: Batch experiment. *Water, Air, & Soil Pollution, 230*, 1–14.

Papita, S., & Chowdhury, S. (2011). Insight into adsorption thermodynamics. In M. Tadashi (Ed.), *thermodynamics.* InTech.

Pereira, S. C., Oliveira, P. F., Oliveira, S. R., Pereira, M. D. L., & Alves, M. G. (2021). Impact of environmental and lifestyle use of chromium on male fertility: Focus on antioxidant activity and oxidative stress. *Antioxidants, 10*, 1365.

Preethi, J., Prabhu, S. M., & Meenakshi, S. (2017). Effective adsorption of hexavalent chromium using biopolymer assisted oxyhydroxide materials from aqueous solution. *Reactive and Functional Polymers, 117*, 16–24.

Rodríguez, F. J., Gutiérrez, S., Ibanez, J. G., Bravo, J. L., & Batina, N. (2000). The efficiency of toxic chromate reduction by a conducting polymer (polypyrrole): Influence of electro polymerisation conditions. *Environmental Science and Technology, 34*, 2018–2023. https://doi.org/10.1021/es990940n

Sall, M. L., Diaw, A. K. D., Gningue-Sall, D., Chevillot-Biraud, A., Oturan, N., Oturan, M. A., & Aaron, J. J. (2017). Removal of Cr (VI) from aqueous solution using electro synthesized 4-amino-3 hydroxynaphthalene-1-sulfonic acid doped polypyrrole as adsorbent. *Environmental Science Pollution and Research, 24*, 21111–21127. https://doi.org/10.1007/s11356-017-9713-y

Sarojini, G., Babu, S. V., Rajamohan, N., Kumar, P. S., & Rajasimman, M. (2021). Surface modified polymer-magnetic-algae nanocomposite for the removal of chromium-equilibrium and mechanism studies. *Environmental Research, 201*, 111626.

Shang, Y., Xu, X., Gao, B., & Yue, O. (2018). Highly selective and efficient removal of fluoride from aqueous solution by Zr-La dual-metal hydroxide anchored bio-sorbents. *Journal of Cleaner Production, 199*, 36–46. https://doi.org/10.1016/j.jclepro.2018.07.162

Sun, W., Zhang, W., Li, H., Su, Q., Zhang, P., & Chen, L. (2020). Insight into the synergistic effect on adsorption for Cr (VI) by a polypyrrole-based composite. *Royal Society of Chemistry Advances, 10*, 8790–8799. https://doi.org/10.1039/C9RA08756G

Tan, Y. Y., Wei, C., Gong, Y. Y., & Du, L. L. (2017). Adsorption of hexavalent chromium onto sisal pulp/polypyrrole composites. *In IOP Conference Series: Material Science Engineering IOP Publishing, 170*, 012007. https://doi.org/10.1088/1757-899X/170/1/012007

Wang, H., Yuan, X., Wu, Y., Chen, X., Leng, L., Wang, H., Li, H., & Zeng, G. (2015). Facile synthesis of polypyrrole decorated reduced graphene oxide-Fe_3O_4 magnetic composites and its application for the Cr (VI) removal. *Chemical Engineering Journal, 262*, 597–606. https://doi.org/10.1016/j.cej.2014.10.020

Wang, J., Wang, X., Zhao, G., Song, G., Chen, D., Chen, H., Xie, J., Hayat, T., Alsaedi, A., & Wang, X. (2018). Polyvinylpyrrolidone and polyacrylamide intercalated molybdenum disulfide as adsorbents for enhanced removal of chromium (VI) from aqueous solutions. *Chemical Engineering Journal, 334*, 569–578.

Wang, H., Hou, L., Shen, Y., Huang, L., He, Y., Yang, W., Yuan, T., Jin, L., Tang, C. J., & Zhang, L. (2020). Synthesis of core-shell UiO-66-poly (m-phenylenediamine) composites for removal of hexavalent chromium. *Environmental Science Pollution Research, 27*, 4115–4126. https://doi.org/10.1007/s11356-019-07070-1

Wang, J., Yu, Q., Zheng, Y., Li, J., Jiao, B., & Li, D. (2022). Adsorption and reduction from modified polypyrrole enhance electrokinetic remediation of hexavalent chromium-contaminated soil. *Environmental Science Pollution Research, 29*, 44845–44861.

Wei, J., Hu, H., Zhang, Y., Huang, Z., Liang, X., & Yin, Y. (2020). In-situ synthesis of poly (m-phenylenediamine) on chitin bead for Cr (VI) removal. *Water, Science and Technology, 82*, 492–502.

Xiang, L., Niu, C. G., Tang, N., Lv, X. X., Guo, H., Li, Z. W., Liu, H. Y., Lin, L. S., Yang, Y., & Liang, C. (2021). Polypyrrole coated molybdenum disulfide composites as adsorbent for enhanced removal of Cr (VI) in aqueous solutions by adsorption combined with reduction. *Chemical Engineering Journal, 408*, 127281. https://doi.org/10.1016/j.cej.2020.127281

Xu, Y., Chen, J., Chen, R., Yu, P., Guo, S., & Wang, X. (2019). Adsorption and reduction of chromium (VI) from aqueous solution using polypyrrole/calcium rectorite composite adsorbent. *Water Research, 160*, 148–157. https://doi.org/10.1016/j.watres.2019.05.055

Yang, D., Chen, Y., Li, J., Li, Y., Song, W., Li, X., & Yan, L. (2022). Synthesis of calcium–aluminum-layered double hydroxide and a polypyrrole decorated product for efficient removal of high concentrations of aqueous hexavalent chromium. *Journal of Colloids and Interface Science, 607*, 1963–1972.

Zhang, L., Niua, W., Sun, J., & Zhou, Q. (2020). Efficient removal of Cr (VI) from water by the uniform fiber ball loaded with polypyrrole: Static adsorption dynamic adsorption and mechanism studies. *Chemosphere, 248*, 126102. https://doi.org/10.1016/j.chemosphere.2020.126102

Zhao, D., Gao, X., Wu, C., Xie, R., Feng, S., & Chen, C. (2016). Facile preparation of amino functionalized graphene oxide decorated with Fe_3O_4 nanoparticles for the adsorption of Cr(VI). *Applied Surface Science, 384*, 1–9.

Zhitkovich, A. (2011). Chromium in drinking water: Sources metabolism and cancer risks. *Chemical Research in Toxicology, 24*, 1617–1629. https://doi.org/10.1021/tx200251t

Zhou, Q., Huang, J., Zhang, X., & Gao, Y. (2018). Assembling polypyrrole coated sepiolite fiber as efficient particle adsorbent for chromium (VI) removal with the feature of convenient recycling. *Applied Clay Science, 166*, 307–317. https://doi.org/10.1016/j.clay.2018.09.031